J Electr Eng Technol.2017; 12(5): 1963-1969
http://doi.org/10.5370/JEET.2017.12.5.1963

ISSN(Print) 1975-0102
ISSN(Online) 2093-7423

# Presentation of a Novel E-Core Transverse-Flux Permanent Magnet Linear Motor and Its Magnetic Field Analysis Based on Schwarz-Christoffel Mapping Method

**Dong-Shan Fu* and Yan-Liang Xu†**

**Abstract** – In order to overcome the manufacturing difficulty of the transverse-flux permanent magnet linear motor (TFPMLM) and enhance its performance much better, a novel TFPMLM with E-core and 3 dimension (3D) magnetic structures is proposed in this paper. Firstly, its basic structure and operating principle are presented. Then the equivalent 2D configuration of the TFPMLM is transformed, so that the Schwarz-Christoffel (SC) mapping method can be used to analyze the motor. Furthermore, the air gap flux density distribution is solved by SC mapping method, based on which, the EMF waveform, no-load cogging force waveform and load force waveform are obtained. Finally, the prototyped TLPMLM is manufactured and the results are obtained from the experiment and 3D FEM, respectively, which are used to compare with those from SC mapping method.

**Keywords**: Transverse-flux permanent magnet linear motor (TFPMLM), Schwarz-Christoffel (SC) mapping method, 3-dimensional finite element method (3D FEM), Prototype experiment

## 1. Introduction

Linear motors are electromechanical devices to produce translational motion and drive the linear load directly without rotary-to-linear mechanical converters, which enjoy the excellent characteristics of high acceleration, high precision and high operating life compared with their counterpart rotary motors. Transverse-flux permanent magnet linear motor (TFPMLM), as one type of linear motors, benefits from the adoptions of both transverse-flux structure and rare earth permanent magnet, so that it has a number of useful features distinguished from other motors, such as high force density, no competition between the space requirement of flux carrying core irons and the space occupied by armature windings. However, the manufacturing process for conventional TFPMLMs is difficult because of the complex structure, and the use of lamination is also difficult [1-3].

Therefore, several configurations of TFPMLMs are proposed to overcome or attenuate the foregoing drawbacks. *Shin* and etc. proposed an double-sided TFPMLM, the armature unit of which is composed of two E-cores equipped face to face, with four coils wound respectively in every side column of E-cores which are connected in series to generate superimposed MMF, the field unit of which consists of two magnets sandwiched between two left sides and two right sides of two E-shape cores respectively [4]. It is noted that the so-called E-core is not a real one, because the middle column of each E-core is only used to fix the two E-cores, with no flux in it. *Li* and *Chau* dashed out one side column of the foregoing E-core and the attached coils and magnet to constitute a C-shaped core TFPMLM [5].

There are some methods already used for analysis and design of TFPMLM, such as theoretical method [6,7], three-dimensional (3D) equivalent magnetic circuit network (EMCN) method coupling on 2D finite element method (FEM) [8,9] and a 3D FEM [10,11]. The theoretical method is adopted only in preliminary design and in understanding apparently relationships between the parameters with low precision and short time. 3D FEM has been proved valuable in the design, performance evaluation and optimization of electrical machine with complex structure such as TFPMLM, with high precision and with the penalty of model establishment difficulty and long computing time. 3D EMCN is a compromise both in precision and consuming time, compared with the other two methods. In fact, the Schwarz-Christoffel (SC) mapping technique is an another analytical-and-numerical method to be used to resolve the air gap field distribution, based on which, the waveforms of electromagnetic force (EMF) and torque (or force in linear motor) and other parameters such as leakage flux, inductance and so on can be reached. The SC method can take into account not only the slotting effects but also the end effects, which are essential for analyzing the linear motors, therefore, this method are widely used in normal permanent magnet linear motor, including the planar one [12] and tubular one[13]. Nevertheless, the SC mapping method has not been used in TFPMLMs so far. It is noted that, the SC mapping method can only be used in electrical machines with 2D magnetic

† Corresponding Author: School of Electrical Engineering, Shandong University, Jinan China. (xuyanliang@sdu.edu.cn)
* School of Electrical Engineering, Shandong University, Jinan China. (sdufuds@mail.sdu.edu.cn)
Received: March 6, 2017; Accepted: June 4, 2017

structure.

The transverse-flux linear motor with real E-core has a higher force-to-weight ratio than that with C-shaped core when it works in reluctance principle [14], as it is the same for TFPMLM. Therefore, in this paper, a novel TFPMLM with E-core and with 3D structure is put forward, the basic structure and operating principle of which is presented. Then the proposed TFPMLM is transmitted into its equivalent 2D configuration, so that the SC mapping method can be used to analysis the motor. Furthermore, the air gap flux density distribution is solved by SC mapping method, based on which, the EMF waveform, no-load cogging force waveform and load force waveform are obtained. Finally, the prototyped TLPMLM is manufactured and the results are obtained from the experiment and 3D FEM, respectively, which are used to compare with those from SC mapping method.

## 2. Structure and Operational Principles of the Novel TFPMLM

Fig. 1 shows the fundamental configuration of the proposed three-phase TFPMLM, which consists of two main parts: the armature one and the field one, as the mover and stator respectively. One armature unit is composed of an E-core and a concentrated coil wound in the middle tooth of the core. One field unit is constituted by two magnets fixed in a nonmagnetic material plate, and magnetized in opposite directions as shown in Fig. 1. Armature units and magnet units are all arranged along the moving direction (z-axis), as shown in Fig. 1(b). Each field unit is electrically separated by 180 degrees and each armature unit is electrically separated by 120 degrees. By applying 3-phase symmetric currents into the 3-phase armature winding (one winding means one coil in Fig. 1), the proposed TFPMLM can work as a 3-phase AC synchronous motor.

As a matter of fact, the proposed TFPMLM supplements a same field unit to *Li*'s motor [5] so that original C-core is changed into E-core in order to attain a higher force-to-weight ratio, higher ability of mechanical equilibrium. At same time, in spite of the adoption of E-core also in *Shin*'s motor [4], the proposed TFPMLM is different from the latter due to the fact as follows: (1) Parallel flux path unlike the latter's serial flux path, (2) One coil taking place of the latter's four coils and (3) The middle column of E-core serves as one portion of magnetic flux path and (4) arrangement of field magnets from two sides of E-core for the latter to the bottom side. As a result, the novel TFPMLM features low copper cost of coil and easy assembly, besides original advantages from the E-core transverse-flux permanent magnet linear motor.

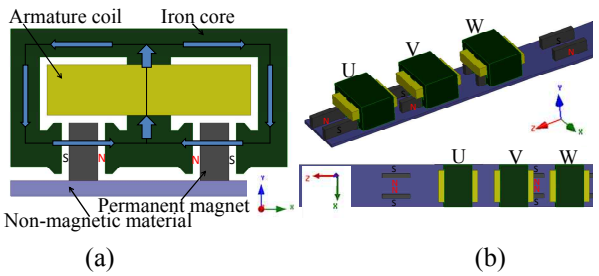


**Fig. 1.** Configuration of the proposed three-phase TFPMLM: (a) one armature and one field units; (b) configuration along the moving direction

## 3. Magnetic Field Analysis of the TLPMLM by SC Mapping Method

SC mapping method is a conformal one that transforms a domain ($\omega$-Plane) with a complex structure to anther domain ($z$-Plane) with a simple structure. The analytical solution is easier to obtain in the $z$-plane, after that mapping the solution back to $\omega$-plane. Simple structure is usually half plane, strips, rectangle, and etc, however the complex structure is usually a polygon. Finding and calculating the correct mapping function, $f(z)$, between the two domains is the key to apply the SC mapping method successfully, and this step can be implemented much easier nowadays with the help of the MATLAB SC Toolbox.

As mentioned above, the SC mapping method is a powerful analytical tool to cope with air gap flux density distribution of the electric machines including the permanent magnet liner motor and then calculate the relative performance such as waveforms of EMF and torque or force. However, the SC mapping method can only be used in 2D situation. Therefore, the proposed TFPMLM, which has a 3D magnetic circuit structure intrinsically, should be first transformed into 2D structure equivalent to its original 3D one, when SC mapping method is adopted in its air gap flux density analysis.

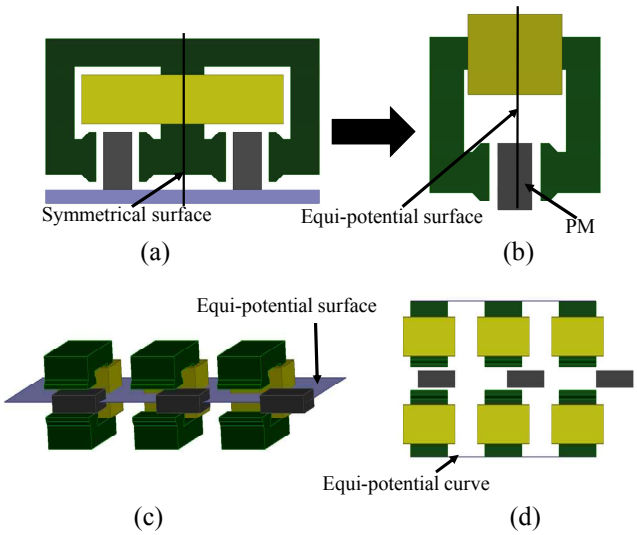


**Fig. 2.** The equivalent transformation of TFPMLM

### 3.1 SC analytical model of the TFPMLM

The procedure of simplifying the 3D structure of the TFPMLM into a 2D model that could be analyzed by the SC mapping method is shown in Fig. 2. Due to the symmetry both in mechanical structure and electro-magnetic structure, the linear motor with E-core shown in Fig. 2(a) can be first converted into the C-shaped configuration shown in Fig. 2(b), then into one shown in Fig. 2(c). Note that there is a symmetrical surface in Fig.2 (a), however there is an Equi-potential surface both in Fig.2 (b) and (c), where the magnetic potential maintains constant. Unroll the motor as shown in Fig. 2(c) based on the Equi-potential surface so that the C-shaped cores is converted into I-shaped ones and then the equivalent 2D structure of the TLPMLM is obtained as shown in Fig, 2(d), where the original equi-potential surface in Fig. 2(c) is expressed by two equi-potential curves.

From Fig. 2(d), It is easier to obtain the SC analysis model of the TFPMLM as shown in Fig. 3, that is, the polygon in $\omega$-Plane, where the dotted lines, *ABCD* and *A'B'C'D'*, serve as the infinite boundaries with a same value of magnetic potential, and both armature winding currents and permanent magnets are expressed equivalently by surface currents. Obviously, it is assumed that the boundaries *ef*, *gh*, *yt*, *rw* are far away from the air gap that they have no effects on air gap flux density.

### 3.2 Air gap field flux Analysis by SC mapping method

As mentioned above, when adopting the SC mapping method to analyze the air gap flux density distribution, the

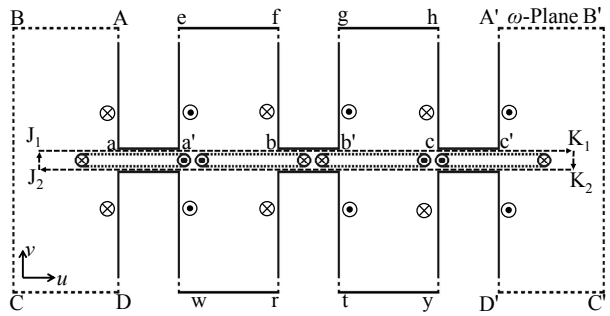


**Fig. 3.** Equivalent SC analysis model of the TFPMLM

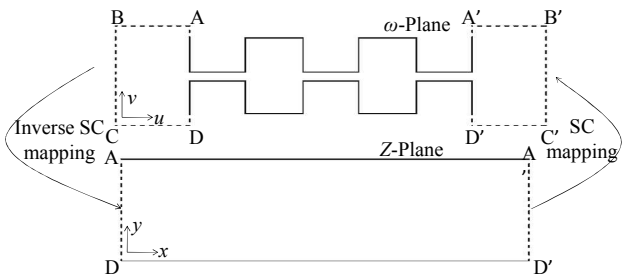


**Fig. 4.** Illustration of SC mapping between different domains in SC method

complex structure ($\omega$-plane) of the SC analysis model shown in Fig. 3 should be transmitted to a simple structure ($z$-plane), where, the flux density can be solved easily in analytical expressions. The processes from $\omega$-plane to $z$-plane is shown in Fig. 4. It can be seen from Fig. 4 that the polygon of TFPMLM's equivalent 2D model in the $\omega$-plane is mapped to a rectangle in the $z$-plane by the inverse SC mapping, which is calculated with the Matlab SC Toolbox. Note that, the infinity boundaries *ABCD* and *A'B'C'D'* in $\omega$-plane correspond to the lines *AD* and *A'D'* of rectangle in $z$-plane respectively, so every point in lines *AD* and *A'D'* of rectangle has vector potential of same value.

The equivalent surface current of permanent magnet in Fig. 3 is segmented into many discrete line currents (the sum of discrete currents is designated as $N_i$), every one of which, $I_i$, can be expressed as:

$$I_i = \left|\boldsymbol{M}\right| h_{\mathrm{PM}} / N_i \tag{1}$$

Where, $h_{\mathrm{PM}}$ and $\boldsymbol{M}$ is the magnetized thickness and magnetization vector of the magnet respectively.

In $z$-plane, the vector potential $A_{i\text{-}z}(x, y)$, generated by line current, $I_i$, in location point $(x, y)$ can be acquired as follows [15]:

$$A_{i-z} = -\frac{\mu_0 I_i}{4\pi}\left[\ln(\cosh\frac{\pi(x-x_i)}{\Delta y} - \cos\frac{\pi(y+y_i)}{\Delta y}) + \ln(\cosh\frac{\pi(x-x_i)}{\Delta y} - \cos\frac{\pi(y-y_i)}{\Delta y})\right] \tag{2}$$

where, $\Delta$y is the height of the rectangle, $(x_i, y_i)$ is the position coordinate where line current $I_i$ is located, and $\mu_0$ is the free space permeability.

From Eq. (2), the flux density ($B_{i\text{-}x}$, $B_{i\text{-}y}$) produced by current $I_i$ in position $(x, y)$ can be expressed as:

$$\begin{cases} B_{i-x} = -\dfrac{\mu_0 I_i}{4\pi}\left(\dfrac{\sin\frac{\pi(y+y_i)}{\Delta y}}{\cosh\frac{\pi(x-x_i)}{\Delta y} - \cos\frac{\pi(y+y_i)}{\Delta y}} + \dfrac{\sin\frac{\pi(y-y_i)}{\Delta y}}{\cosh\frac{\pi(x-x_i)}{\Delta y} - \cos\frac{\pi(y-y_i)}{\Delta y}}\right) \\ B_{i-y} = \dfrac{\mu_0 I_i}{4\pi}\left(\dfrac{\sinh\frac{\pi(x-x_i)}{\Delta y}}{\cosh\frac{\pi(x-x_i)}{\Delta y} - \cos\frac{\pi(y+y_i)}{\Delta y}} + \dfrac{\sinh\frac{\pi(x-x_i)}{\Delta y}}{\cosh\frac{\pi(x-x_i)}{\Delta y} - \cos\frac{\pi(y-y_i)}{\Delta y}}\right) \end{cases} \tag{3}$$

Since the flux density ($B_{i\text{-}x}$, $B_{i\text{-}y}$) in position $(x, y)$ of $z$-plane has been expressed as Eq. (3), corresponding flux

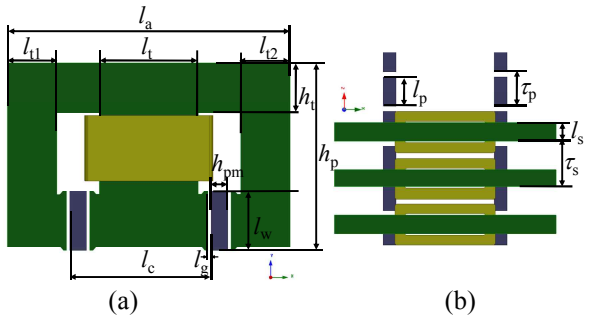


**Fig. 5.** Structural parameter labels of the TFPMLM(a) *x-y* coordinate and (b) *x-z* coordinate

density ($B_{i\text{-}u}$, $B_{i\text{-}u}$) in position ($u$, $v$) of $\omega$-plane can be obtained from Eq. (4).

$$B_{i\text{-}u} + jB_{i\text{-}v} = \frac{B_{i\text{-}x} + \mathrm{i}\, B_{i\text{-}y}}{\overline{f'(z)}} \tag{4}$$

where, $f'(z)$ is the derivative of the SC mapping function $f(z)$, and $\overline{f'(z)}$ is the conjugate form of complex $f'(z)$, which can also be computed by calling the Matlab SC Toolbox.

However, as mentioned above, the magnetic vector potentials in the *AD* and *A'D'* should keep invariant during SC mapping. Therefore, to obtain the field solution in the rectangle of *z*-plane, an additional line current $I_{ai}$ at infinity should be introduced according to the uniqueness theorem and imaging method [15].

Considering the superposition effect of current $I_{ai}$, The flux density in the $\omega$-plane produced by $I_i$ expressed in Eq. (4) becomes as follows:

$$B_{i\text{-}u} + jB_{i\text{-}v} = \left(\frac{B_{i\text{-}x} + j\left(B_{i\text{-}y} + \dfrac{\Delta A_{i\text{-}z}}{\Delta x}\right)}{\overline{f'(z)}}\right) \tag{5}$$

where, $\Delta A_{i\text{-}z}$ is the difference value of the magnetic vector potential in the rectangle sides, *AD* and *A'D'*, calculated by Eq. (2), when without considering the boundary conditions, $\Delta x$ is the breadth of the rectangle.

As mentioned above, the air gap flux density, ($B_{i\text{-}u}$, $B_{i\text{-}v}$), of the TFPMLM produced by current $I_i$ is obtained from Eq. (5), therefore, it is easy to obtain the air gap flux density ($B_u$, $B_v$) of the TFPMLM when excited only by the magnets according to the superposition principle, shown as Eq. (6).

$$B_u + jB_v = \sum_i^{N_i} B_{i-u} + j\sum_i^{N_i} B_{i-v} \tag{6}$$

## 4. Calculation of EMF and Force of the TFPMLM

The air gap flux density obtained above is integrated along with *aa'*, *bb'* and *cc'* (shown in Fig. 3) respectively in order to acquire the three phase flux linkages, $\Psi_{abc}$ (combined expression of $\Psi_a$, $\Psi_b$ and $\Psi_c$) of the TFPMLM as follows:

$$\Psi_{abc} = 2Nl_w \begin{bmatrix} \int_{aa'} B_v \,\mathrm{d}v \\ \int_{bb'} B_v \,\mathrm{d}v \\ \int_{cc'} B_v \,\mathrm{d}v \end{bmatrix} \tag{7}$$

where, $N$ is the number of phase winding turns (here, $N$ is the coil turns), and $l_w$ is the pole arc depth as shown in Fig. 5.

So, the three phase EMFs, $e_{abc}$ can be obtained by the derivative of the flux linkages $\Psi_{abc}$ with respective time $t$ as follows:

$$e = -\frac{\partial \Psi}{\partial t} = -\frac{\partial \Psi}{\partial \Delta z}\frac{\partial \Delta z}{\partial t} = -\frac{\partial \Psi}{\partial \Delta z}\upsilon \tag{8}$$

where, $\upsilon$ is the translator speed.

The force of a region in the magnetic field can be calculated by integrating Maxwell stress tensor on a boundary of the region. As shown in Fig. 3, the lines $J_1K_1$, $K_1K_2$, $K_2J_2$, $J_2J_1$, are chosen as the integral paths for calculating the force of the motor. So the force can be expressed as:

$$\begin{aligned} F_u = \frac{2l_w}{\mu_0}\Big(&\int_{J_1K_1} B_u B_v \,\mathrm{d}u - \int_{J_2K_2} B_u B_v \,\mathrm{d}u - \int_{J_2J_1} \frac{B_u^2 - B_v^2}{2}\mathrm{d}v \\ &+ \int_{K_1K_2} \frac{B_u^2 - B_v^2}{2}\mathrm{d}v\Big) \end{aligned} \tag{9}$$

Eq. (8) and Eq. (9) are expressions of the EMF and cogging force of the TLPMLM, because the air gap flux density is generated only by magnet excitation. When at load, the air gap flux density is a resultant one, which can also be calculated from Eq. (6) where the excitations results not only from equivalent current of magnet, but phase currents, and the load force can also be acquired from Eq. (9).

## 5. 3D FEM and Experiment Verification

For the purpose of verification of SC mapping method when used in TFPMLM's analysis of the air gap flux density and then the resultant EMF and force, a three-phase prototyped TFPMLM is fabricated, whose structure parameter labels and the specifications are shown in Fig. 5 and Table 1 respectively. The turn number of phase winding, $N$, is 300. The magnet of NdFeB is adopted with remanent flux density of 1.3T and coercive force of 890kA/m.

**Table 1.** Specification of the prototyped TFPMLM

| Parameters | Value | Parameters | Value |
|---|---|---|---|
| $l_a$ [mm] | 86 | $l_g$ [mm] | 1 |
| $l_t$ [mm] | 30 | $l_w$ [mm] | 18 |
| $l_{t1}$ [mm] | 15 | $h_{pm}$ [mm] | 5 |
| $l_{t2}$ [mm] | 15 | $l_p$ [mm] | 11.5 |
| $h_t$ [mm] | 15 | $\tau_p$ [mm] | 13.5 |
| $h_p$ [mm] | 57 | $\tau_s$ [mm] | 18 |
| $l_c$ [mm] | 43 | $l_s$ [mm] | 7 |

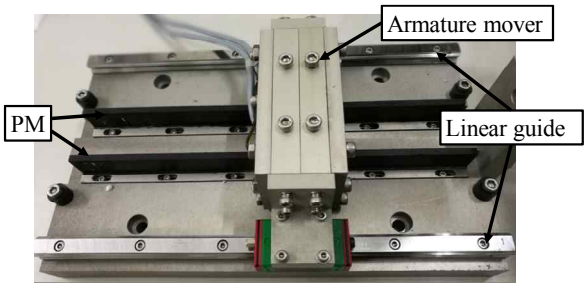


**Fig. 6.** The prototyped TFPMLM

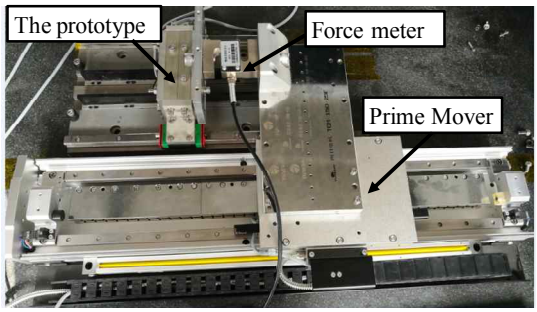


**Fig. 7.** The test platform of the prototyped motor

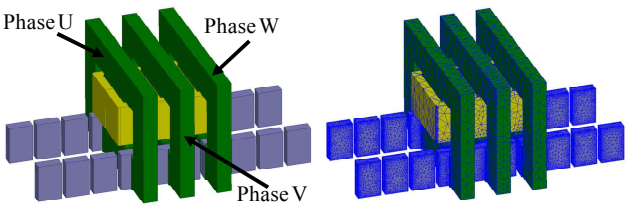


**Fig. 8.** The 3D FEM model and its mesh model (a) 3D solid mode and (b) 3D mesh model

The prototyped TFPMLM is shown in Fig. 6, which features a short armature mover of only three units, and a longer field stator. The prototyped TFPMLM is tested, 3D FEM-based and SC mapping-based calculated for its air gap flux density distributions, EMF waveforms, force waveforms when it is at no-load and at load. The test platform is shown in Fig. 7, which consists mainly of the prototyped TFPMLM, force meter and prime liner motor, and the prime linear motor is used to push the mover of the prototyped motor, the force meter which is used to measure the force output of the prototyped motor, is sandwiched

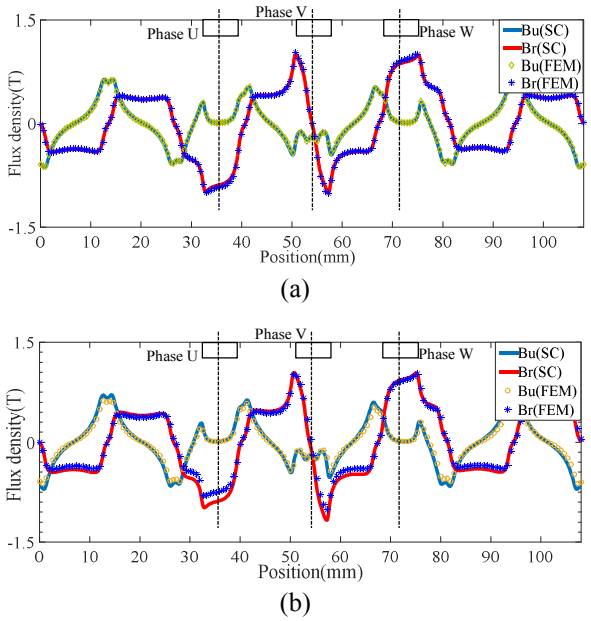


**Fig. 9.** The air-gap flux density distribution results from SC mapping method and 3D FEM (a) at no load and (b) at load with $I_U$=3A, $I_V$=$I_W$=0A

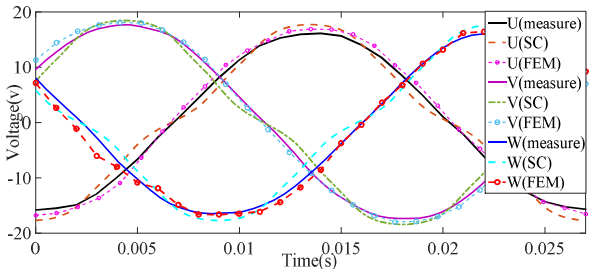


**Fig. 10.** EMF results from SC mapping method, 3D FEM and experiment when the prototype motor moves in a constant speed of 1 m/s

between the movers of prototyped motor and the prime liner motor. The 3D FEM model and its mesh model are shown in Fig. 8, where, only the mesh expressions of the main parts of the motor, those are E-cores, coils and magnets, are given.

Assumed that armature mover of the prototyped TFPMLM is situated in such location that the Phase V is aligned with the q-axis of the field stator as shown in Fig. 8.

The air gap field flux distributions of the prototyped TLPMLM are obtained by SC mapping method and 3D FEM respectively as shown in Fig. 9, under the following two conditions: (1) at no load, means that the three phase windings are open-circuited, and (2) at load when Phase U is supplied with direct current of 3A, but other two windings are open circuited, that is, $I_U$=3A, $I_V$=$I_W$=0A. It can be seen from Fig. 9 that the results from SC mapping method and 3D FEM are much coincided with each other, except a little difference for the $B_r$ component when at load,

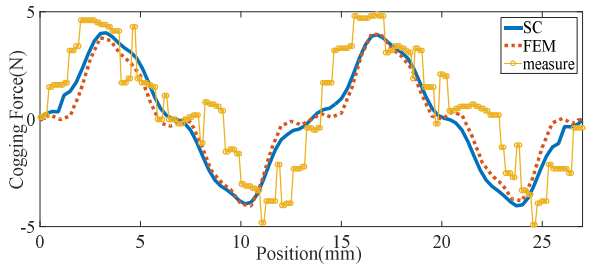


**Fig. 11.** The cogging force comparison obtained from SC mapping method, 3D FEM and experiment

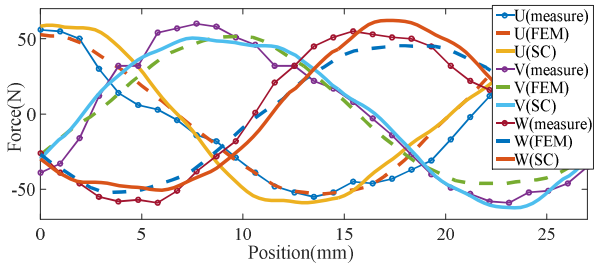


**Fig. 12.** The load force comparison obtained from SC mapping method, 3D FEM and experiment

especially in air gap range of phase U-core.

The three-phase on-load EMF waveform results based on SC mapping method, 3D FEM and experiment are shown in Fig. 10 respectively, when the prototyped motor moves in a constant speed of 1m/s. From Fig. 10, it can be seen that, the EMF waveforms from SC mapping method are in agreement much better with those from 3D FEM and experiment.

The prime linear motor drive the prototyped motor, so that the motor moves in a constant speed of 1m/s, then the force meter shows the cogging force when three-phase windings of the prototyped motor with no current supply. On the other hand, the cogging force can also be obtained from SC mapping method and 3D FEM. The cogging force waveform comparison from these three methods is given in Fig. 11. Do the same comparison as that of the cogging force, but one of the three-phase windings of the prototyped motor is supplied with direct current of 3A respectively, with other two-phase winding open-circuited, and the three force waveforms are displayed in the same figure as shown in Fig. 12. It can be seen from Fig. 11 and Fig. 12, which the no-load cogging force waveforms obtained from SC mapping method, 3D FEM and experiment respectively are in agreement with each other to some extent, as is the same for the force results when at load.

Therefore, the SC mapping method is proved to be an effective and convenient one when used to analyze the TFPMLM, by comparing the results of air gap flux density distribution, EMF waveform, and force waveform when the motor is at no-load and at load, based on SC mapping method, 3D FEM and experiment, respectively.

## 6. Conclusion

An novel transverse-flux permanent magnet linear motor (TFPMLM) with E-cores, is proposed, which enjoys special advantages of low copper cost of coil, easy assembly and no lateral force besides the common characteristics for this type of linear motor such as high efficiency, high force density and no competition between magnetic setup and electrical setup. The Schwarz–Christoffel (SC) mapping method is adopted conveniently to analyze the motor's air gap field flux distribution. According to the obtained air gap flux density distribution, the no-load EMF waveforms, no-load cogging force waveform and load force waveforms are obtained. All the results from SC mapping method are much in agreement with those from 3D FEM and experiment for a prototyped TLPMLM. It should be noted that, due to the adaptability of SC mapping method only in 2D structure, the proposed TLPMLM which features a 3D structure, should first be transmitted equivalently into its 2D configuration.

## Acknowledgements

This work was supported by Department of Science and Technology of Shandong Province of China (2015 ZDXX0601B01)

## References

[1] J. Chang and D. Kang, "Development of transverse flux linear motor with permanent-magnet excitation for direct drive application," *IEEE Trans. Magn*, Vol. 5, No. 41, pp. 1936-1939, 2005.

[2] S. D. Joao and V. Mauricio, "Transverse flux machine: What for?," *IEEE Multidisciplinary Eng. Edu. Ma*, Vol. 2, No. 1, pp. 4-6, 2007.

[3] M. Zhao, Q. Wang, J. Zou and G. Wu, "Development and analysis of tubular transverse flux machine with permanent-magnet excitation," *IEEE Trans. Ind. Electron*, Vol. 59, No. 5, pp. 2198-2207, May 2012.

[4] Jung-Seob Shin, Takafumi Koseki and Houng-Joong Kim, "Proposal of Double-Sided Transverse Flux Linear Synchronous Motor and a Simplified Design for Maximum Thrust in Nonsaturation Region," *IEEE Trans. Magn*, Vol. 49, No. 7. pp. 4104-4108, 2013.

[5] Wenlong Li and K.T. Chau, "Design and Analysis of a Novel Linear Transverse Flux Permanent Magnet Motor Using HTS Magnetic Shielding," *IEEE Transactions on Applied Superconductivity*, Vol. 20, No. 3, pp. 1106-1109, Jun. 2010.

[6] Shin Jung-Seob, Takafumi Koseki and Kim Houng-Joong, "Proposal and design of short armature core double-sided transverse flux type linear synchronous motor," *IEEE Trans. on Magn*, Vol. 48, No.11, pp.

3871-3874, Nov. 2012.
[7] Jung-Seob Shin, Ryuji Watanabe, Takafumi Koseki and Houng-Joong Kim, "Practical design approach of a transverse flux linear synchronous motor for compact size, small mover weight, high efficiency, and low material cost," *IEEE Trans. on Magn*, Vol. 51, No. 3, pp. 1-4, March 2015.
[8] Junghwan Chang, Dohyun Kang, Jiyoung Lee and Jungpyo Hong, "Development of transverse flux linear motor with permanent-magnet excitation for direct drive applications," *IEEE Trans. on Magn*, Vol. 41, No. 5, pp. 1936-1939, May 2005
[9] Ji-Young Lee, Ji-Won Kim, Jung-Hwan Chang, Si-Uk Chung, Do-Hyun Kang and Jung-Pyo Hong, "Determination of parameters considering Magnetic nonlinearity in solid core transverse flux linear motor for dynamic simulation," *IEEE Trans. on Magn*, Vol. 44, No. 6, pp. 1566-1569, June 2008.
[10] A. S. Abd-Rabou, H. M. Hasanien and S. M. Sakr, "Design development of permanent magnet excitation transverse flux linear motor with inner mover type," *IET Eledtr. Power Appl*, Vol. 4, No. 7, pp. 559-568, May 2009.
[11] Rashed Meer, H. M. Hasanieu and A. J. Alolah, "Design development of two phase transverse flux linear with permanent-magnet excitation," *in Proceedings of 2015 IEEE International Electric Machines and Drives Conference*, pp. 1818-1813, May 2015.
[12] D. C. J. Krop, E. A. Lomonova, and A. J. A. Vandemput, "Application of Schwarz-Christoffel mapping to permanent-magnet linear analysis," *IEEE Trans. on Magn*, Vol. 44, No. 3, pp. 352-357, March 2008.
[13] B. L. J. Gysen, E. A. Lomonova, and etc., "Analytical and numerical techniques for solving laplace and poisson equations in a tubular permanent magnet actuator: Part 2. Schwarz-Christoffel mapping," *IEEE Trans. on Magn*, Vol. 44, No. 7, pp. 1761-1767, July 2008.
[14] Xinglong Li and Ernest A. Mendrela. "Optimization of Construction of Linear Switched Reluctance Motor with Transverse Magnetic Flux," *in Proceedings of 2008 IEEE Region 5 Conference*, pp. 1-5, April 2008.
[15] Lizhan Zeng, Xuedong Chen, Xiaoqing Li, Wei Jiang and Xin Luo, "A Thrust Force Analysis Method for Permanent Magnet Linear Motor Using Schwarz–Christoffel Mapping and Considering Slotting Effect, End Effect, and Magnet Shape," *IEEE Trans. Magn*, Vol. 51, No. 9, pp. 1-9, Sept 2015.

**Dong-Shan Fu** He received received B.S degree in Electrical engineering and automation from the School of Information and Electrical Engineering, China University of Mining and Technology, Xuzhou, China, in 2013. He is currently pursuing the Ph. D. degree in School of Electrical Engineering at the Shandong University, China. His research interests are design and analysis for permanent-magnet machine and special structural machine.

**Yan-Liang Xu** He received B.S and MSc in Electrical machines from Shandong University of Technology, Jinan, China, in 1989 and 1994, respectively. He received the PhD. degree in electrical machines in Shenyang University of Technology, Shenyang, China, in 2001. Currently he is a Professor in School of Electrical Engineering, Shandong University. He is the head of the Institute of Electrical Machine. His research interests are electrical machines especially permanent magnet electrical machine and special electrical machine.